Statistical evaluation of the performance of free-space-optical link affected by optical turbulence with gamma-gamma distribution through time series generated by simulation

J. A. López-Leyva[a,*], A. Arvizu-Mondragon[b], J. Santos-Aguilar[b], and F. J. Mendieta-Jimenez[b]
[a]*Centro de Enseñanza Técnica y Superior Universidad,*
Camino a Microondas Trinidad s/n. Km. 1, Moderna Oeste, 22860 Ensenada, B.C., México.
[b]*Department of Applied Physics. CICESE Research Center. Baja California, México,*
Carret. Ens. -Tij. 3918, Zona Playitas, Ensenada, B.C. 22860, México.
[*]*e-mail: josue.lopez@cetys.mx*

Received 05 July 2020; accepted 26 September 2020

In this article, the statistical evaluation of the performance of FSO links subject to dynamic fluctuations of atmospheric optical turbulence that affect the instantaneous value of the received optical power is presented. We reproduce this temporal domain effect with time series generated by simulation considering the optical turbulence as a stochastic process with Gamma-Gamma probability distribution. Also, a phase screen was used in order to observe the impact that optical turbulence has over the optical information field's spatial phase. With our simulations, it is possible to get the two most essential performance parameters required for the practical implementation of FSO links. We obtained the mean signal-to-noise ratio (SNR) and the mean bit error rate (BER) of FSO links affected by optical turbulence with Gamma-Gamma distribution, where the results show that the mean SNR and mean BER are adequately modified according to the atmospheric turbulence levels, *e.g.*, ≈ 1.4 dB for $\sigma_R^2 = 0.33$ and ≈ 0.36 dB for $\sigma_R^2 = 1$. Thus, the methodology presented in this paper may be readily used to design and implement real-world FSO links.

Keywords: Simulated series; atmospheric turbulence; Free-Space-Optical.

PACS: 92.60.hk; 07.05.Tp; 84.40.Ua

DOI: https://doi.org/10.31349/RevMexFis.67.146

1. Introduction

Nowadays, Free-Space-Optical (FSO) communication links are used for short distances in the Local Area Network or Metropolitan Area Network. They are also being used for long-distance links, particularly for conventional satellite and quantum security applications [1-3]. However, the process of designing optical links in the classical and quantum domain requires, in addition to the traditional optical power budget, to take into account diverse phenomena that affect the overall performance, such as the atmospheric turbulence [4]. The atmospheric turbulence modifies the refractive index of air masses depending on the pressure and temperature value in such a way that the optical field's diverse parameters may be affected by this phenomenon. Among these parameters are its phase, amplitude, state of polarization, orbital angular momentum, and also some phenomena such as the quantum entanglement [5,6]. In general, the FSO link is designed and characterized, firstly, in the laboratory environment, then, a real implementation at different distances is needed for different applications [7,8]. However, the characterization of such links still lacks a rigorous prior analysis regarding atmospheric turbulence. Although there are some experimental proposals for atmospheric turbulence chambers, they present important limitations and trade-offs such as 1) static or sometimes dynamic design with reduced configuration parameters, 2) reduced limit of emulated link distances, and 3) reduced control of atmospheric turbulence levels, among others [9,10]. Several mathematical algorithms simulate the effects of atmospheric turbulence over an optical field [11-14]. However, to the best of our knowledge, such algorithms do not determine the actual received optical power (measured in Watts) for the different possible regimes of atmospheric turbulence based on characteristics of physical devices. This document presents a technique for the design and statistical evaluation of FSO links based on the simulation of the optical information signal affected by different atmospheric turbulence levels. For this purpose, we generate by simulation a data time series with a Gamma-Gamma probability density function that allows modeling optical turbulence from low to high turbulence regimes. We organized our paper as follows: Section 2 presents some theoretical aspects of atmospheric turbulence and its effect over the optical power and the spatial phase of the received signal. Section 3 presents the results obtained in our simulations. Finally, Sec. 4 presents the conclusion and important aspects of future work.

2. Theoretical background

2.1. Atmospheric turbulence theory

A parameter commonly used to indicate the level of atmospheric turbulence is the scintillation index σ_I^2 related to the irradiance of the optical field traveling through the free space

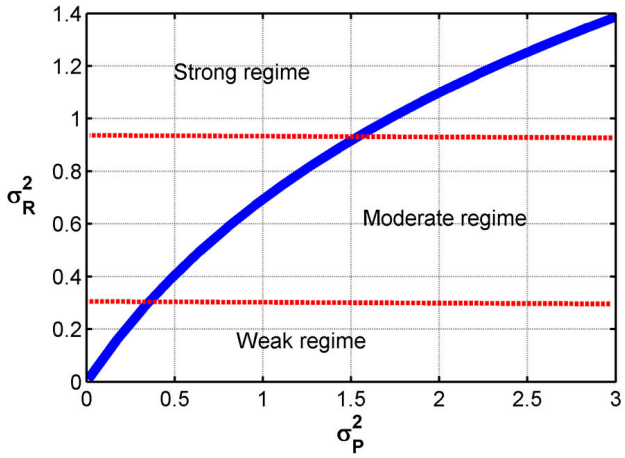

FIGURE 1. Relationship between σ_P^2 and σ_R^2 for several turbulence levels.

channel. But as the optical power and the irradiance are related, one instead may use the power scintillation index σ_P^2 for a particular distance link (L) using Eq. (1):

$$\sigma_P^2 = \frac{\langle P_{Rx}^2(L)\rangle}{\langle P_{Rx}(L)\rangle^2} - 1, \tag{1}$$

where $P_{Rx}(L)$ denotes the optical power affected by turbulence at a distance $L(m)$ from the optical transmitter, $\langle\rangle$ is the ensemble average (sample mean), and, the log power variance (Rytov variance) σ_R^2 is related to σ_P^2 as $\sigma_P^2 = \exp(\sigma_R^2) - 1$, considering that $\sigma_P^2 \approx \sigma_R^2$ for $\sigma_R^2 \ll 1$, *i.e.*, applicable for weak turbulence regime, as Fig. 1 shows. Thus, the σ_R^2 value is described for long-distance links (*i.e.*, for plane wavefront) as Eq. (2) [15]:

$$\sigma_P^2 = \sigma_R^2 = 1.23 C_n^2 k^{7/6} L^{11/6}. \tag{2}$$

On the other hand, for spherical wavefront, $\sigma_P^2 = 0.4\sigma_R^2 = 0.5 C_n^2 k^{7/6} L^{11/6}$. Here, $C_n^2(m^{-2/3})$ is the index of refraction structure parameter, $k = 2\pi/\lambda$ is the optical wavenumber (m), λ is the wavelength, and $L(m)$ is the propagation path length between transmitter and receiver systems. Also, C_n^2 may be considered constant for a given condition of optical turbulence in horizontal links. However, if the weather conditions change, the value of C_n^2 will change accordingly [15]. We will see this effect more clearly in vertical links where the C_n^2 value will depend on each atmospheric layer through which the optical beam travels. In our paper, we calculate the C_n^2 value considering only the transmitter and receiver locations in a horizontal link for a fixed condition of optical turbulence (*i.e.*, we defined the full effect of the turbulence through the atmosphere as a black box).

As Eq. (1) showed, σ_P^2 parameter depends on the receiver optical power $P_{Rx}(L)$ affected by the stochastic variations of the optical turbulence in addition to diverse (static) losses introduced by the free-space optical channel. As Eq. (1) showed, σ_P^2 parameter depends on the receiver optical power $P_{Rx}(L)$ according to the free space loss (L_s) (*i.e.* Free-Space Path Loss law is shown in Eq. (3)). Although other kinds of losses are present in an FSO link (*e.g.*, beam divergence, weather conditions, pointing) and laws, as Beer's law. Hence, $P_{Rx} = P_{Tx} L_s$ [16].

$$L_s = \left(\frac{\lambda}{4\pi L}\right)^2. \tag{3}$$

The stochastic behavior of atmospheric optical turbulence is commonly described using a lognormal probability density function (pdf) due to its relative simplicity. However, this description is valid just for low to medium turbulence values. On the other hand, there are other more complex probability density functions, such as the called Gamma-Gamma, whose results are valid for weak to strong turbulence levels. The Gamma-Gamma (f_{GG}) pdf describes turbulence as a function of small and large-scale variations. Equation (4) shows the relation of f_{GG} with P_{Rx} with α and β parameters being the effective number of small-scale and large-scale eddies of the scattering environment, respectively [16]. Commonly, Eq. (4) is related to the irradiance (W/m^2), but considering the active area (m^2) of a suitable photodetector, Eq. (4) can be expressed using the optical power received.

$$f_{GG}(P_{Rx};\alpha,\beta) \propto \frac{2(\alpha\beta)^{(\alpha+\beta)/2}}{\Gamma(\alpha)\Gamma(\beta)} \times P_{Rx}^{(\alpha+\beta)/2-1} k_{\alpha-\beta}(2\sqrt{\alpha\beta P_{Rx}}), \tag{4}$$

where $\Gamma(\cdot)$ is Gamma function, and $K_a(\cdot)$ is the modified Bessel function of second kind of order a. The parameters of the Gamma-Gamma function are related to the Rytov variance using Eqs. (5) and (6) under the assumption of plane wave and negligible inner scale, which corresponds to long propagation distance and small detector area [17].

$$\alpha = g(\sigma_R) = \left\{\exp\left[\frac{0.49\sigma_R^2}{(1+1.11\sigma_R^{12/5})^{7/6}}\right] - 1\right\}^{-1}, \tag{5}$$

$$\beta = h(\sigma_R) = \left\{\exp\left[\frac{0.51\sigma_R^2}{(1+0.69\sigma_R^{12/5})^{5/6}}\right] - 1\right\}^{-1}. \tag{6}$$

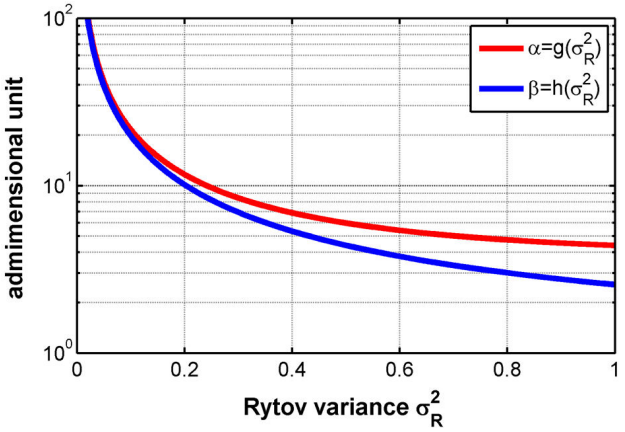

FIGURE 2 . Relationship between σ_R^2 and α, β.

For instance, if $\sigma_R^2 = 0.3$ implies the values of $\alpha = 8.42$ and $\beta = 6.91$. Figure 2 shows the behavior of $g(\sigma_R)$ and $h(\sigma_R)$ for the range $0 < \sigma_R^2 \leq 1$, from weak to strong turbulence regimes.

2.2. Data affected by simulated atmospheric turbulence

To simulate the temporal behavior of the optical channel, we generate a time-series for the data-signal affected by different atmospheric turbulence levels that satisfy a Gamma-Gamma distribution based on [18]. Also, in our simulations, we take into account the static attenuation on the optical field when it travels through the free space optical channel according to Beer-Lambert law, which is described as $\tau(\lambda, L)$, where τ is the transmittance or atmospheric transmission. In particular, two stochastic processes are used to describe the small-scale and large-scale turbulence, which are described by the Gamma functions, $\Gamma(\alpha)$ and $\Gamma(\beta)$, respectively. Therefore, $x_{k+1}(\alpha)$ and $y_{k+1}(\beta)$ describe the temporal data (*i.e.*, an ensemble of many particular values, k) that satisfies the functions $\Gamma(\alpha)$ and $\Gamma(\beta)$ from Eqs. (7) and (8) [18].

$$x_{k+1}(\alpha) = \frac{\left\{ x_k\tau_c + \Delta t + \left[\frac{\Delta t(\xi_k^2-1)}{2\alpha}\right] + \left(\frac{2x_k\tau_c\Delta t}{\alpha}\right)^{1/2}\xi_k \right\}}{1+\Delta t,} \tag{7}$$

$$y_{k+1}(\beta) = \frac{\left\{ y_k\tau_c + \Delta t + \left[\frac{\Delta t(\xi_k^2-1)}{2\beta}\right] + \left(\frac{2y_k\tau_c\Delta t}{\beta}\right)^{1/2}\xi_k \right\}}{1+\Delta t.} \tag{8}$$

Here, ξ_k is a normal uncorrelated White Gaussian Noise (WGN) process, τ_c is the correlation time between samples, Δt is the sampling time, and k is the particular sample. In this way, in Eqs. (7) and (8) are used to calculate the normalized received optical power, $\overline{P_{Rx}}(\alpha)$ and $\overline{P_{Rx}}(\beta)$, respectively, as shown in Eqs. (9) and (10). Since the stochastic processes described in Equations (7) and (8) are independent, the multiplication of both processes generates a time-series signal that satisfies a Gamma-Gamma distribution, $\overline{P_{Rx}}(\alpha, \beta)$, which is also normalized as Eq. (10) shows.

$$\overline{P_{Rx}}(\alpha) \propto x_{k+1}(\alpha), \quad \overline{P_{Rx}}(\beta) \propto y_{k+1}(\beta), \tag{9}$$

$$\overline{P_{Rx}}(\alpha, \beta) \propto x_{k+1}(\alpha) y_{k+1}(\beta). \tag{10}$$

Finally, the optical signal received affected by simulated atmospheric turbulence, as well as the attenuation introduced by free space, is described in Eq. (11), where P_{rx} is the denormalized form of the complete expression at the right side of Eq. (11).

$$P_{rx} = P_{Tx}\tau(\lambda, L)\overline{P_{Rx}}(\alpha, \beta). \tag{11}$$

It is convenient to note that Eq. (11) is the optical power received affected only by the turbulence and optical channel attenuation according to Beer-Lambert law. However, in a real-world environment, it is required to take also into account the photodetector responsivity $\Re$[A/W], so Eq. (11) is modified as:

$$Y_{Rx} = \Re[P_{Tx}\tau(\lambda, L)\overline{P_{Rx}}(\alpha, \beta) \otimes h + z], \tag{12}$$

where Y_{Rx} is the photocurrent at the receiver, h is the impulse response of an ideal low-pass filter representing the limited bandwidth of photoreceiver, and z is any front-end noise in the photoreception stage ($e.g.$, thermal, among others) [19]. All the parameters are time-dependent, except $\Re$. For coherent detection schemes used in quantum communication links, the Standard Quantum Limit (SQL) imposes that z is determined by shot noise.

2.3. Phase fluctuation induced by atmospheric turbulence

Another essential aspect to consider in FSO links is the phase fluctuation in a spatial region of the detector. The atmospheric turbulence modifies the phase of the signal in different regions of the wavefront that can affect the communications link's performance, particularly for coherent detection schemes. There are various phase drifts in an FSO link (*e.g.*, optical phase drift caused by phase noise); however, we will only consider spatial phase fluctuation because the other phase noises are not caused by turbulence. It is possible to determine the power spectrum of these phase fluctuations using Eq. (13), representing a thin phase screen [20-22].

$$\varphi_n(K) = 0.033C_n^2k^2Lx^{-11/3} = 0.033r_0^{-5/3}K^{-11/3}, \tag{13}$$

where K is the transverse coordinate, considering that a single atmospheric layer (multiple atmospheric layers simulation requires a high-end computer system) based on the aperture diameter D_G of the telescope used. r_0 is the wavefront coherence diameter describing the spatial correlation of phase fluctuations in the receiver plane due to random inhomogeneities in the atmosphere's refractive index. In our case, $r_0 = (k^2C_n^2L)^{-3/5}$, and it is constant because we consider just a single atmospheric layer. In particular, the phase screen does not modify the amplitude; in fact, the optical phase is

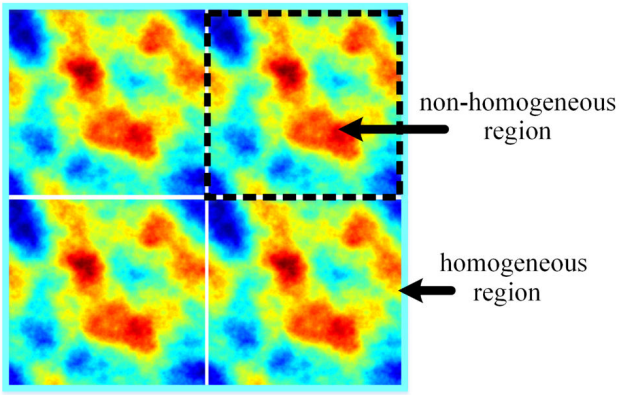

FIGURE 3. Individual non-homogeneous phase screen as part of a large homogeneous phase screen.

the only parameter affected. It is important to mention that Eq. (13) is based on Discrete Fourier Transform (DFT), which means that the phase screen is periodic. This argument imposes a wrong hypothetical scenario of small non- homogeneous regions inside a homogeneous large region (see Fig. 3) that have to be considered for large region analysis taking into account D_G and r_0 parameters.

2.4. Mean Signal to Noise Ratio for atmospheric turbulence link

Evaluating the performance of an FSO link affected by atmospheric turbulence are used parameters such as the electrical Signal-to-Noise Ratio (SNR) and the Bit Error Rate (BER) at the output of the photoreceiver for different modulation schemes. Equation (14) shows the SNR without taking into account the atmospheric turbulence, where h is the Planck's constant $v = c/\lambda$, and B is the bandwidth of the photoreceiver used [21]. Also, Eq. (14) is only considering the SQL; in another way, the thermal noise has to be considered.

$$SNR_0 = \frac{i_s^2}{\sigma_N^2} = \frac{\langle Y_{Rx}^2 \rangle}{\sigma_N^2} \propto \sqrt{\frac{P_{Tx}\tau(\lambda, L}{2hvB}}\,. \tag{14}$$

However, since the optical power received is affected by dynamical and random atmospheric turbulence, it is not possible to calculate the SNR for specific power received. Therefore, the mean SNR $(E[SNR])$ measurement is required, as Eq. (15) shows [21]:

$$E[SNR] = \frac{SNR_0}{\sqrt{\left(\frac{P_{Tx}\tau(\lambda,L)}{\langle P_{Tx}\tau(\lambda,L)\overline{P_{Rx}}(\alpha,\beta)\rangle}\right) + \sigma_P^2(D_G)SNR_0^2}}, \tag{15}$$

where $\sigma_P^2(D_G)$ is the power variance in the plane of the detector, D_G is the aperture diameter of the receiver (*i.e.*, first lens of the telescope). In the same way, $\sigma_P^2(D_G) = \sigma_P^2(0, L + L_f)$, where L_f is the focal length. In particular, $\sigma_P^2(D_G) = 0$ means that atmospheric effects are not present in the link. Also, σ_P^2 can be related to σ_I^2 (flux irradiance variance). In particular, if the terms, $P_{Tx}\tau(\lambda, L)$ and $\langle P_{Tx}\tau(\lambda, L)\overline{P_{Rx}}(\alpha, \beta)\rangle$ are considered with same mean values, then:

$$\left(\frac{P_{Tx}\tau(\lambda, L)}{\langle P_{Tx}\tau(\lambda, L)\overline{P_{Rx}}(\alpha, \beta)\rangle}\right) = 1\,. \tag{16}$$

Therefore, the Eq. (15) can be rewritten as Eq. (17) shows, which is related to Eqs. (5-6)

$$E[SNR] = \frac{SNR_0}{\sqrt{1 + \sigma_P^2(D_G)SNR_0^2}} = \frac{SNR_0}{\sqrt{1 + [\exp(\sigma_P^2) - 1](D_G)SNR_0^2}}. \tag{17}$$

On the other hand, E[SNR] can also be related to the phase perturbations described by Eq. (13). In particular, calculating the C_n^2 (based on a particular atmospheric turbulence level), it is possible to determine the σ_R^2 value and, next, determine the α and β parameters by Eqs. (5-6). Finally, in order to calculate the mean Bit Error Rate ($E[BER]$) for OOK modulation and Direct Detection (DD), it is necessary to normalize the received power using $x = P_{rx}/\langle P_{rx}\rangle$ in Eq. (18). Here, $p(x)$ is the Gamma- Gamma probability density function that represents the atmospheric turbulence for different levels [21].

$$E[BER] = \frac{1}{2}\int_0^\infty p(x) erfc\left(\frac{E[SNR]x}{2\sqrt{2}}\right) dx \approx \frac{1}{2}\sum_{i=1}^{\infty} p(x_i) erfc\left(\frac{E[SNR]x_i}{2\sqrt{2}}\right). \tag{18}$$

In particular, Eq. (18) is presented as a continuous integration of the power received affected by atmospheric turbulence, however; it is possible to modify the mathematical expression to optimize the computational simulation based on narrow bins (i) that represent certain optical power measured.

3. Results and analysis

In order to determine the temporal behavior of a hypothetical optical signal received, some technical settings were established, such as $P_{Tx} = 500$ mW, $L = 10,000$ m, $\lambda = 1550$ nm, $\tau_c = 20$ ms, 5×10^5 samples with $\Delta t = 10^{-4}$ s and bit rate at 350 KHz. All parameters are variable in

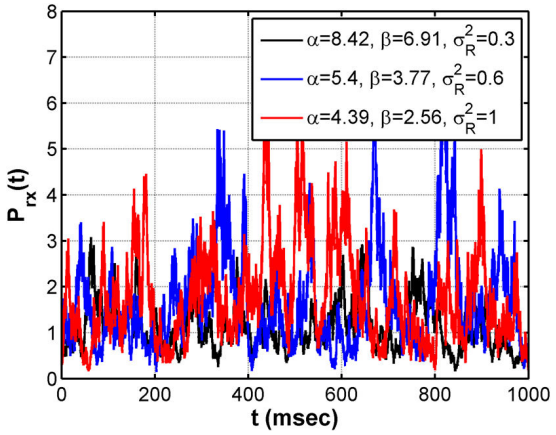

FIGURE 4. Simulated Gamma-Gamma Time-series signal for different turbulence regimes.

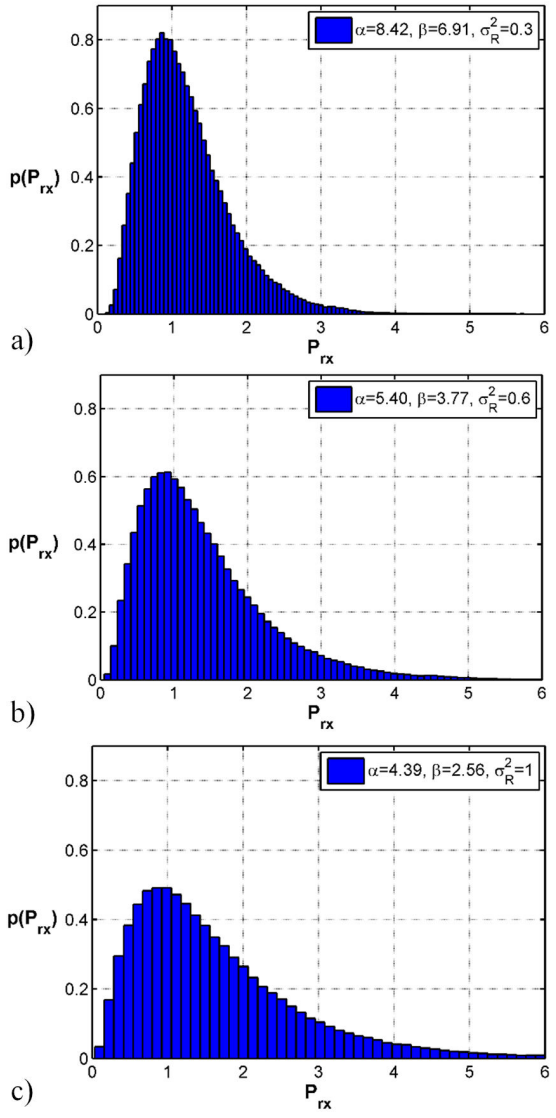

FIGURE 5. Probability density function of the simulated Gamma-Gamma signal for different turbulence regimes a) Weak, b) Moderate, c) Strong.

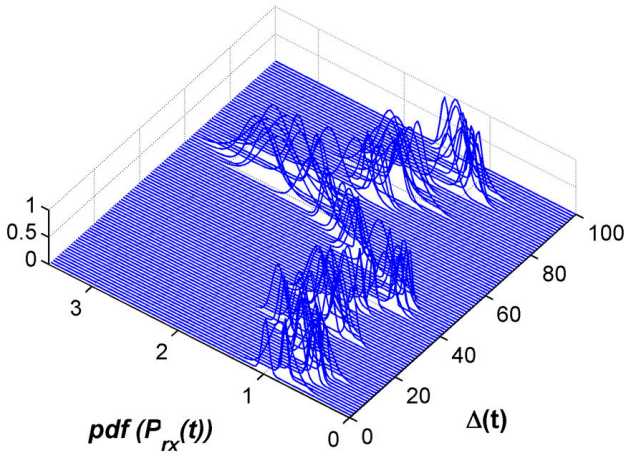

FIGURE 6. Probability density function of the simulated Gamma-Gamma signal received.

the simulation, and, in fact, some parameters are simplified or normalized to show general results. Figure 4 shows the optical signal on the receiver side based on Eqs. (3) and (11) for different turbulence regimes. Besides, Fig. 5 shows the distribution of numerical data of the optical signal received considering weak, moderate, and strong atmospheric turbulence regime with particular values for σ_R^2, α, and β. These distributions have a Gamma-Gamma probability density function shape. In particular, $C_n^2 = 2.22\times10^{-16}$ m$^{-2/3}$ for $\sigma_R^2 = 0.3$, and C_n^2 can be calculated for a particular turbulence regime. Thus, the results showed in Figs. 4 and 5 can be modified according to atmospheric turbulence levels (*i.e.*, modifying C_n^2 parameter) based on the Rytov variance and Gamma-Gamma parameters.

Figure 5 shows the distribution of the samples and, regarding the strong turbulence regime, the mean value of P_{Rx} is less than the other regimes because P_{Rx} presents more fluctuations in the samples ensemble, *i.e.*, the optical power received is increased for those samples that had less optical power in the weak and moderate turbulence regimes.

Thus, for a strong turbulence regime, the probability is increased for all samples that represent high power received $(P_{Rx} > 2)$, and decreased for $P_{Rx} = 1$. On the other hand, Fig. 6 shows the probability density function considering a fixed ensemble data related to $\Delta t = 10$ ms in order to visualize the particular behavior of the optical signal related to the temporal variation using a turbulence level condition close to the moderate turbulence regimes. It can be seen that the density function does not change; that is, it remains Gaussian, so it can be interpreted that the optical state has not changed due to the non-linearity of the atmospheric channel.

Figure 7 shows the simulated phase screen considering the parameters mentioned and an aperture diameter $D_G = 5$ cm based on Eq. (13). The results show that the phase screen imposes a phase variation added to the phase noise of the optical signal for a particular spatial position on the receiver side. The maximum and minimum variations are 8 and -8 radians, respectively, for $C_n^2 = 2.22 \times 10^{-16}$ m$^{-2/3}$ (*i.e.*,

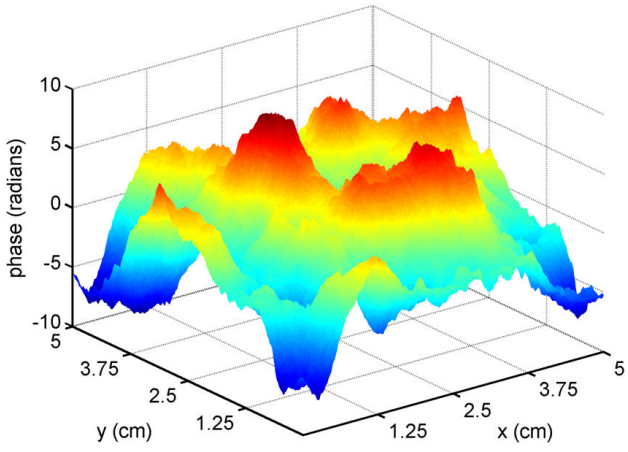

FIGURE 7. Simulated phase screen of the signal received. $D_G = 5$ cm.

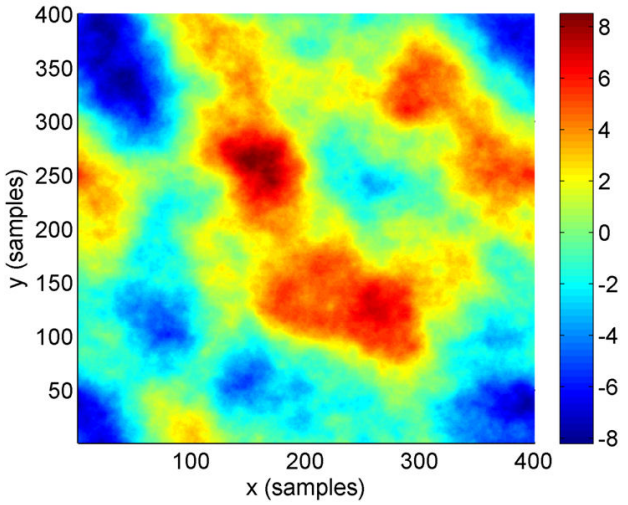

FIGURE 8. Simulated phase screen of the signal received. Wavefront phase aberrations due to Kolmogorov turbulence, $D_G = 5$ cm.

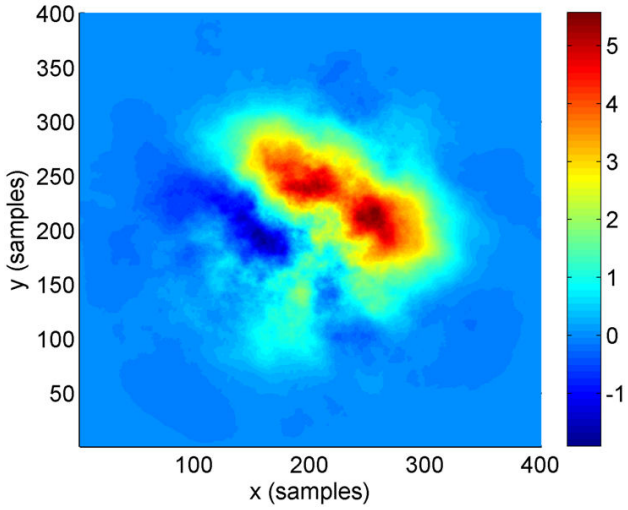

FIGURE 9. Simulated spatial phase distribution considering a single phase screen, $D_G = 5$ cm.

meaning a moderate turbulence level, although this parameter can be modified). In order to clarify, the maximum and minimum variations do not imply generalized phase changes; in fact, the mean phase variation is less than 0.5 radians. It is important to clarify that the phase screen showed is a random numerical result according to (13), *i.e.*, in general, different representations of phase screen can be generated maintaining the maximum and minimum phase variation similar. Also, Fig. 7 is represented using the physical dimension of the receiver aperture diameter, while Fig. 8 shows the same results in a different representation considering the spatial samples based on the sample resolution, *i.e.*, 400 samples for x and y-axis, which means that 1 sample is equivalent to 0.0125 cm. This resolution is optimal in order to characterize small and large eddies present in the turbulence medium.

Therefore, considering a Gaussian beam transmitted through the atmospheric turbulence and a single-phase screen, both represented before, it is possible to obtain a spatial phase representation as Fig. 9 shows. It is important to mention that the results can vary because they are evaluated based on random variables. Nevertheless, the results generated are very useful for FSO communication systems. Besides Fig. 10 shows the theoretical and numerical results

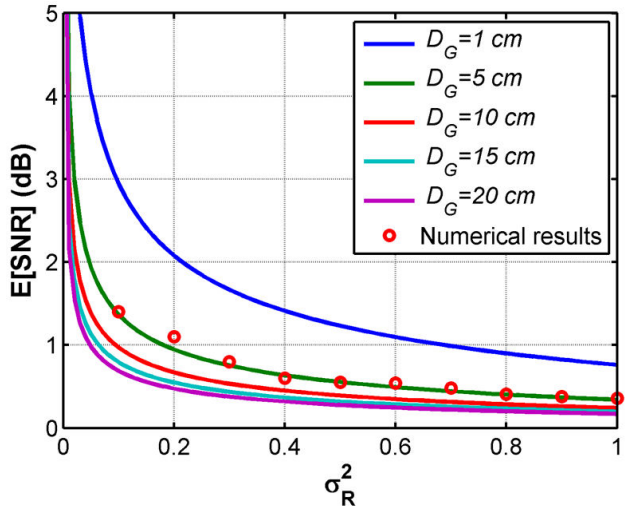

FIGURE 10. Mean SNR for different D_G values and numerical results for mean SNR for simulated series-time data affected by atmospheric turbulence.

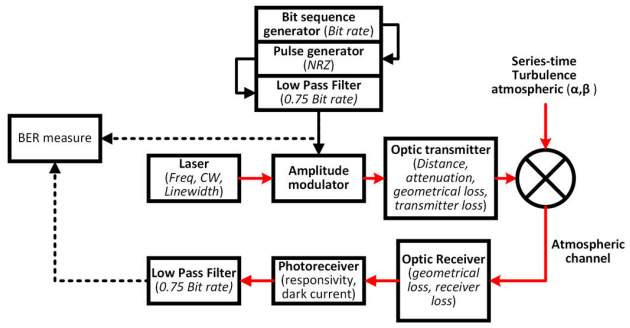

FIGURE 11. Block diagram used for simulation.

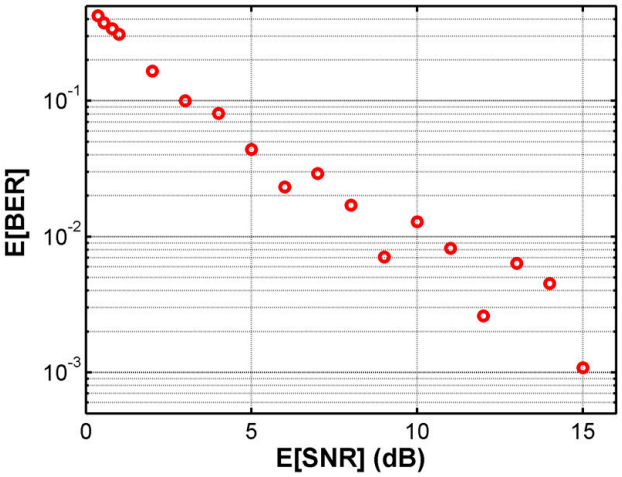

FIGURE 12. Numerical results for mean BER of the series-time for different mean SNR.

for the mean SNR parameter considering different atmospheric turbulence levels (from weak to strong turbulence) and aperture diameters. In particular, the σ_P^2 values for each simulated series-time showed in Fig. 4 are affected by different D_G values, as Eq. (17) showed. Therefore, the mean SNR is reduced for stronger atmospheric turbulence levels, *i.e.*, 1.4 dB for $\sigma_R^2 = 0.33$ and 0.36 dB for $\sigma_R^2 = 1$. The latter, due to the increasing variation of the values generated and showed in Fig. 5. Besides it is important to mention that the mean SNR is also increased based on the aperture diameter. Hence, the atmospheric turbulence characterization in an FSO link has to be performed based on a particular and well-known photodetector and passive optical devices. The SNR0 value was considered constant (*i.e.*, 10 dB), which is related to Eq. (14).

Figure 11 shows the block diagram used in order to obtain the simulation results considering particular values for the different subsystems of the overall communication system. The simulation was performed using a homologated Matlab script based on the VPI photonics program, although the OptiSystem program is also useful. In particular, a bit sequence generator at 350 Kbps (related to $\tau_c = 20$ ms) is used, a pulse generator based on Non-return-to-zero (NRZ) and Low Pass Filter ($f_c = 0.7 \times$ bit rate) produces the input digital signal to the amplitude modulator. Concerning the optical source, a CW laser (500 mW) at $\lambda = 1550$ nm ($v = 193.41$ THz) and $\Delta v = 1$ MHz is used. Thus, the electrical input signal modulates the optical signal. Next, the simulation considers some features of the optical transmitter, such as distance link (10 Km), attenuation (2.3 dB/Km), geometrical losses (10 dB), and transmitter losses (3 dB). The photoreceiver has a responsivity of 1 A/W and a dark current of 10 nA. Regarding the atmospheric channel, a multiplying point permits the introduction of the series-time turbulence based on Gamma-Gamma distribution function.

Finally, Fig. 12 shows the results of $E[BER]$ for different $E[SNR]$ values based on Fig. 11. Remember that according to Eq. (17), the mean SNR value depends on some parameters such as D_G, σ_R^2, and SNR_0. In this case, $D_G = 5$ cm, $\sigma_R^2 = 1$, and SNR_0 are modified in relation to particular photodetectors. However, it is possible to use a particular photodetector and vary the Rytov variance, *i.e.*, a particular mean SNR value can mean a combination of different parameter values presented in the free space link and receiver scheme. In fact, the results simulated based on series-time data affected by atmospheric turbulence described for Gamma-Gamma function are closely related to the theoretical results showed in [21].

4. Conclusions

The accurate characterization of the optical signal transmitted through the atmospheric channel is necessary in order to offline research the possible effects in a future hypothetical FSO link to improve the overall performance. Thus, simulated series-time signals affected by atmospheric turbulence were generated based on two stochastic processes described by a Gamma probability density function in order to calculate the performance of a particular FSO link. The simulation permits to visualize an optical signal affected by different atmospheric turbulence regimes, *i.e.*, from $\sigma_R^2 = 0.1$ to $\sigma_R^2 = 1$, and calculate the mean SNR and mean BER using a time-interval of 1 second. The simulation can be expanded to large time-intervals according to the performance parameters required (*e.g.*, Bit Error Rate), transmission rates used in particular FSO links, and scheme modulations (*e.g.*, Quadrature Amplitude Modulation (QAM), Phase Shift Keying (PSK), among others). Also, the spatial phase was simulated for particular σ_R^2 value, although it is possible to modify the atmospheric condition parameters to determine the correct spatial phase perturbation. In particular, the correlation time value used is directly obtained based on the temporal covariance function for a particular condition of the FSO link, *i.e.*, the time value for $1/e$ of the normalized temporal covariance function is the correlation time. This condition is described based on the distance of link, Rytov variance, and the transverse wind speed for Taylor's frozen-turbulence hypothesis [21]. This means that the simulation proposed is suitable to analyze only the FSO links that satisfy the conditions mentioned. Finally, the numerical results regarding the mean SNR and mean BER for different atmospheric turbulence regimes are highly related to the theoretical performance. In fact, if this simulation proposal is used for the design and proof of concept of FSO links previous to the real implementation, it is necessary to provide technical details of each optical and optoelectronic device to increase the accuracy of the numerical results.

1. A. K. Mohammad and M. Uysal, M., Survey on Free Space Optical Communication: A Communication Theory Perspective, *Commun. Surv. Tut.* **16** (2014) 2231. https://doi.org/10.1109/comst.2014.2329501
2. J. G. Perez, *et al*., Ethernet FSO Communications Link Performance Study Under a Controlled Fog Environment, *Commun. Lett.* **16** (2012) 408. https://doi.org/10.1109/LCOMM.2012.012412.112072
3. Z. Ghassemlooy, *et al*., Performance Analysis of Ethernet/Fast-Ethernet Free Space Optical Communications in a Controlled Weak Turbulence Condition, *J. Lightwave Technol.* **30** (2012) 2188. http://dx.doi.org/10.1109/JLT.2012.2194271
4. H. Kaushal and G. Kaddoum, Optical Communication in Space: Challenges and Mitigation Techniques, *Commun. Surv. Tut.* **19** (2017) 57. https://doi.org/10.1109/comst.2016.2603518
5. L. B. Pedireddi and B. Srinivasan, Characterization of atmospheric turbulence effects and their mitigation using wavelet-based signal processing, *Trans. Commun.* **58** (2010) 1795. http://dx.doi.org/10.1109/TCOMM.2010.06.090194
6. C. Gopaul and R. Andrews, The effect of atmospheric turbulence on entangled orbital angular momentum states, *New J. Phys.* **9** (2007) 1. https://doi.org/10.1088/1367-2630/9/4/094
7. E. Diamanti, *et al.*, Practical challenges in quantum key distribution, *npj Quantum Inf.* **2** (2016) 1. https://doi.org/10.1038/npjqi.2016.25
8. K. Tsukamoto, *et al*. The case for free space, *Microw. Maga.* **10** (2009) 84. https://doi.org/10.1109/MMM.2009.933086
9. H. Kaushal, *et al.*, Experimental Study on Beam Wander Under Varying Atmospheric Turbulence Conditions, *Photon. Tech. Lett.* **23** (2011) 1691. https://doi.org/10.1109/lpt.2011.2166113
10. S. Rajbhandari, *et al.*, Experimental Error Performance of Modulation Schemes Under a Controlled Laboratory Turbulence FSO Channel *J. Lightwave. Technol.* **33** (2015) 244. https://doi.org/10.1109/JLT.2014.2377155
11. R. Pernice, *et al.*, Indoor free space optics link under the weak turbulence regime: measurements and model validation, *IET Commun.* **9** (2015) 62. http://dx.doi.org/10.1049/iet-com.2014.0432
12. A. Lylova, *et al.*, A new method of the real-time atmospheric turbulence modeling, *ICLO* (2016) 4. https://doi.org/10.1109/lo.2016.7549767
13. F. Yıldız and H. Kurt, Numerical studies of laser beam propagation with phase screen method using Non- Kolmogorov atmospheric turbulence, *SPIE* (2017) 10425. https://doi.org/10.1117/12.2278129
14. A.R. Camboulives, *et al.*, Statistical and temporal irradiance fluctuations modeling for a ground-togeostationary satellite optical link, *Appl. Opt.* **57** (2018) 709. https://doi.org/10.1364/AO.57.000709
15. M. Niu, *et al.*, Terrestrial Coherent Free-Space Optical Communication Systems, *Opt. Commun.* (2012) 169. http://dx.doi.org/10.5772/48284
16. H. G. Sandalidis, *et al.*, Optical Wireless Communications with Heterodyne Detection Over Turbulence Channels with Pointing Errors, *J. Lightwave Technol.* **27** (2009) 4440. http://dx.doi.org/10.1109/JLT.2009.2024169
17. N. Wang and J. Cheng, Moment-based estimation for the shape parameters of the Gamma-Gamma atmospheric turbulence model, *Opt. Exp.* **18** (2010) 12824. https://doi.org/10.1364/OE.18.012824
18. D. Bykhovsky, Simple Generation of Gamma, Gamma-Gamma, and K Distributions with Exponential Autocorrelation Function, *J. Lightwave Technol.* **34** (2016) 2106. https://doi.org/10.1109/JLT.2016.2525781
19. A. Garcia-Zambrana, *et al.*, On the Capacity of FSO Links over Gamma- Gamma Atmospheric Turbulence Channels Using OOK Signaling, *J. Wireless Com. Network.* (2010) 1. https://doi.org/10.1155/2010/127657
20. V. I. Tatarski, *Wave Propagation in a Turbulent Medium* (1961) 285.
21. L. C. Andrews and R. L. Phillips, Laser Beam Propagation through Random Media, *SPIE* (2005)
22. F. Dios, *et al.*, Temporal analysis of laser beam propagation in the atmosphere using computer-generated long phase screens, *Opt. Exp.* **16** (2008) 2206. https://doi.org/10.1364/OE.16.002206